Ionics (2020) 26:1673–1680
https://doi.org/10.1007/s11581-019-03296-8

ORIGINAL PAPER

Preparation and electrochemical properties of $LiFePO_4/C-Li_4Ti_5O_{12}$ composites

Shihong Yang[1] · **Zhijiang Liu**[1] · **Xuetian Li**[1] · **Zhongcai Shao**[1]

Received: 6 September 2019 / Revised: 28 September 2019 / Accepted: 5 October 2019 / Published online: 5 December 2019

Abstract

$LiFePO_4/C-Li_4Ti_5O_{12}$ composite electrode materials were synthesized by blending $LiFePO_4/C$ and $Li_4Ti_5O_{12}$ materials then calcining at 500 °C for 14 h. The effects of different composite ratios on the phase structure and electrochemical properties of $LiFePO_4/C-Li_4Ti_5O_{12}$ composite cathode materials were investigated. The results showed that the structure of $LiFePO_4/C$ and $Li_4Ti_5O_{12}$ in the composite prepared by the simple blending method did not change. XRD shows only the characteristic peaks of these two substances and no characteristic peaks of other crystal impurities. When the recombination ratio was 8:2 (LPF-8), the obtained composite material had fine particles and uniform size. The initial discharge capacity at 0.1C rate is 151.56 mAh g^{-1} at the voltage of 1.0–4.2 V. After 100 cycles, the capacity retention rate was 97.3% which exhibited more outstanding electrochemical performance than samples with other composite ratios.

Keywords $LiFePO_4/C-Li_4Ti_5O_{12}$ · Lithium-ion battery · Cathode material

Introduction

The using of $Li_4Ti_5O_{12}$ as anode for lithium-ion batteries was first proposed by Canadian scholar K. Zaghib [1–3]. Later, some people also used $Li_4Ti_5O_{12}$ as anode material [4–7]. It is found that [8–11] the structure of $Li_4Ti_5O_{12}$ does not change during charging and discharging. The $Li_4Ti_5O_{12}$ material has the advantages of high charge-discharge efficiency, where the diffusion coefficient of Li^+ is ten times higher than carbon anode [12–15]. It has faster charging characteristics, more cycles, and safer use of the new-generation lithium-ion battery [16–20].

The low migration ability of Li^+ in the material is a bottleneck that inhibits development of $LiFePO_4$ cathode materials [21–24]. At present, the mature methods such as carbon coating, particle size reduction, and metal element doping are used to improve the low electronic conductivity of $LiFePO_4$ and the small diffusion coefficient of lithium ions [25–29]. Studies have shown that [30–34] doping high-valence Ti^{4+} in $LiFePO_4$ can cause V_{Li} defects in the material, thereby improving Li^+ migration ability and electrochemical performance of the material. $Li_4Ti_5O_{12}$ and $LiFePO_4$ materials were selected as research objects, which were prepared by solid-phase method. The two materials were simply blended in different proportions to obtain $LiFePO_4/C-Li_4Ti_5O_{12}$ composites. The structure, morphology, and electrochemical properties of $LiFePO_4/C-Li_4Ti_5O_{12}$ composite cathode materials were investigated.

Experiment

Preparation of $LiFePO_4/C$

$LiOH·H_2O$ and $FePO_4$ with a molar ratio of 1.05:1 were mixed as raw materials, and ethanol was used as a dispersing agent. The ball-to-material ratio was 15:1 in a planetary ball mill. After ball milling for 10 h, it was dried in a vacuum-drying oven. The dried mixture was pre-sintered at 350 °C for 4 h under N_2 atmosphere and then calcined at 700 °C for 12 h to obtain $LiFePO_4/C$ material.

Preparation of $Li_4Ti_5O_{12}$

$LiOH·H_2O$ and TiO_2 with a molar ratio of 4.08:5 were mixed as raw materials, ethanol was used as dispersing agent, and the ball-to-material ratio was 15:1 in a planetary ball mill. The ball

---

✉ Zhijiang Liu
shaozc@sylu.edu.cn

[1] School of Environmental and Chemical Engineering, Shenyang Ligong University, ShenYang 110159, Liaoning Province, People's Republic of China

was ground for 10 h, and the ground powder was placed in a vacuum-drying oven. The dried mixture was pre-sintered at 450 °C for 4 h under N_2 atmosphere and then calcined at 800 °C for 12 h to obtain $Li_4Ti_5O_{12}$ material.

Preparation of $LiFePO_4$/C-$Li_4Ti_5O_{12}$ composite

The $LiFePO_4$/C and $Li_4Ti_5O_{12}$ materials were placed in a planetary ball mill with ethanol as dispersing agent. The ratio of the ball to the material was 15:1. After ball milling for 10 h, the material was dried and transferred into a porcelain boat. Under nitrogen protection, the mixture was pre-sintered at 300 °C for 5 h and then calcined at 500 °C for 14 h to obtain a sample of $LiFePO_4$/C-$Li_4Ti_5O_{12}$. $LiFePO_4$/C-$Li_4Ti_5O_{12}$ composite cathode materials with different composite ratios were synthesized from $LiFePO_4$/C and $Li_4Ti_5O_{12}$ at a mass ratio of 9:1, 8:2, 7:3, and 6:4, respectively, which were identified as LFP-9, LFP-8, LFP-7, and LFP-6.

Assembly of button battery

The active material, polyvinylidene fluoride and acetylene black were taken at a mass ratio of 80:10:10, and NMP was mixed uniformly to adjust the slurry. Finally, the slurry was coated on an aluminum foil and dried in a vacuum oven at 80 °C for 20 h. After the sample was dried, it was punched into a disk having a diameter of 17.2 mm by a punching machine as a positive electrode sheet. The lithium sheet was a negative electrode, the Celgard 2400 porous polypropylene was used as separator, and the electrolyte was an organic solution of EC, DMC, and DEC (volume ratio EC:DMC:DEC = 1:1:1) of 1 M $LiPF_6$. A button battery was assembled in the glove box for testing.

Results and discussion

Structure analysis of materials

Figure 1 shows the XRD patterns of $LiFePO_4$/C and $Li_4Ti_5O_{12}$, which are consistent with the standard spectrum. There is no impurity phase in diffraction peaks, indicating that the prepared $LiFePO_4$/C sample is a pure-phase olivine structure. After the carbon source is added, the carbon exists in the material at amorphous state. The $Li_4Ti_5O_{12}$ material is a spinel structure. Compared with the XRD of $LiFePO_4$/C material, each diffraction peak of $Li_4Ti_5O_{12}$ material has higher intensity, sharper peak shape, and narrower half width, which indicate that the $Li_4Ti_5O_{12}$ sample has better crystallinity than $LiFePO_4$/C material.

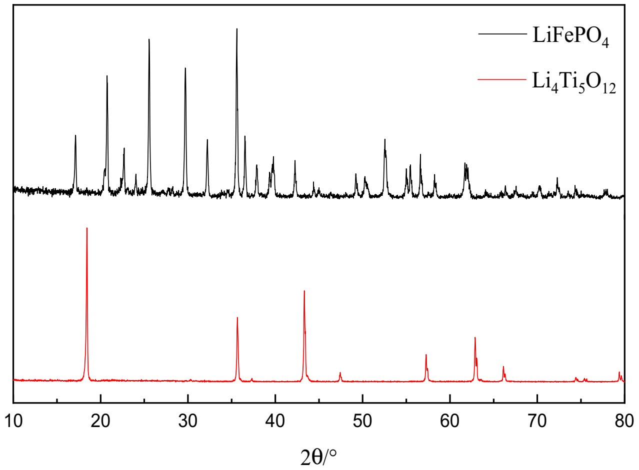

Fig. 1 The XRD patterns of $LiFePO_4$ and $Li_4Ti_5O_{12}$ samples

Figure 2 shows that the crystal structures of the two materials are not changed after the simple blending of $LiFePO_4$/C and $Li_4Ti_5O_{12}$. The diffraction peaks are superposed on each other according to the blending ratio, and no impurity peak appears. With the gradual increase of the proportion of $Li_4Ti_5O_{12}$ in the composite, the characteristic diffraction peak of $Li_4Ti_5O_{12}$ is increasingly obvious.

Morphological analysis of materials

As shown in Fig. 3(A, a), $LiFePO_4$/C is a secondary particle with an average particle size of about 18 μm. Each secondary particle is composed of many primary particles, and the $LiFePO_4$/C sample reflected by the primary particles has an olivine structure. It can be seen from Fig. 3(B, b) that $Li_4Ti_5O_{12}$ material is composed of primary particles of spindle type, and the average particle diameter is 7 μm. These particles are not agglomerated into secondary particles, and the dispersibility is well. The $Li_4Ti_5O_{12}$ sample has small particle

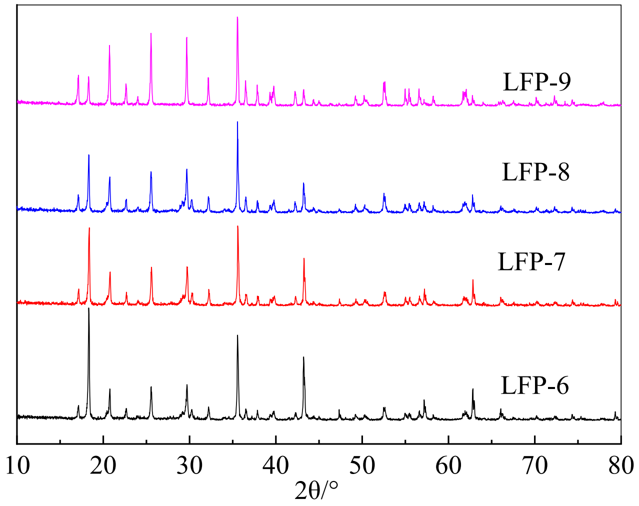

Fig. 2 The XRD patterns of LFP-6, LFP-7, LFP-8, and LFP-9 samples

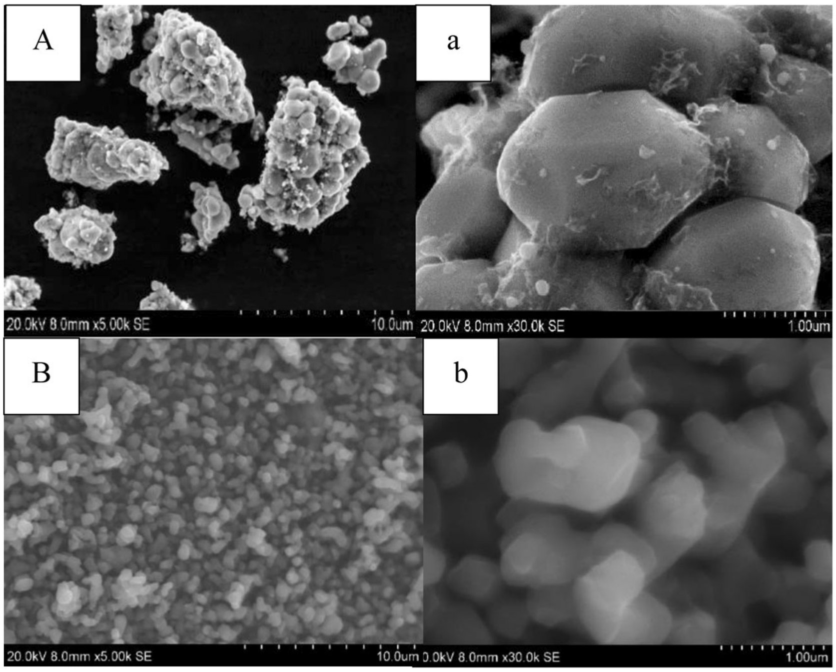

Fig. 3 SEM of $LiFePO_4/C$ (A, a) and $Li_4Ti_5O_{12}$ (B, b) samples

size and large surface area, which facilitates the deintercalation of Li^+.

As illustrated in Fig. 4, the morphology of the $LiFePO_4/C-Li_4Ti_5O_{12}$ composite obtained after blending is not as good as that of the single $LiFePO_4/C$, which may be due to the long-time grinding of the blended material. After that, the morphology of the olivine particles of $LiFePO_4/C$ material is destroyed. The smaller particles of $Li_4Ti_5O_{12}$ are all adhered to the surface of $LiFePO_4/C$ particles and a part of the encapsulated $LiFePO_4/C$ particles agglomerate. From Fig. 4(A, a), we find that $LiFePO_4/C$ particles are not completely covered by $Li_4Ti_5O_{12}$ appeared in the LFP-9 material. This is because the proportion of $Li_4Ti_5O_{12}$ in the blended material is low and the effect of complete coating cannot be achieved. This will affect the electrochemical performance to some extent. We can also know that the particles in LFP-8 material are smaller than the particles of LFP-9, LFP-7, and LFP-6 materials and the particle size is average. $Li_4Ti_5O_{12}$ cannot only completely coat $LiFePO_4/C$ but be dispersed in $LiFePO_4/C$ particle gap with a tight filling state, which is conducive to the transfer of lithium ions. It has a positive effect on the improvement of electrochemical performance.

Figure 5 shows that the four elements of Ti, P, O, C, and Fe are uniformly distributed in the samples. Combined with the SEM and XRD patterns of LFP-8, the synthesized material is a pure $LiFePO_4/C-Li_4Ti_5O_{12}$ with uniform element distribution.

Electrochemical performance analysis of materials

Charge and discharge test of materials

Figure 6 shows $LiFePO_4/C$ samples tested for charge and discharge at a voltage range of 2.0–4.8 V at 0.1, 0.2, 0.5, 1, and 2C, respectively. As can be seen from Fig. 6, the $LiFePO_4/C$ sample exhibits a charge and discharge characteristic platform at about 3.6 V/3.4 V, which corresponds to the redox reaction of Fe^{3+}/Fe^{2+}. The specific discharge capacities at 0.1, 0.2, 0.5, 1, and 2C rates are 128, 121, 108, 72, and 39 mAh g^{-1}, respectively. The corresponding coulombic efficiencies are 98.1, 96.7, 96.6, 91.4, and 84.4%, respectively. It can be seen from the data that as the charge-discharge rate increases, the discharge-specific capacity and discharge efficiency of the $LiFePO_4/C$ sample decrease rapidly, and the charge-discharge platform gradually becomes unapparent. The potential difference between the platforms and the polarization of the battery increases, the discharge efficiency decreases, resulting in the worse rate performance of the battery.

Figure 7 shows the first charge-discharge curves of LFP-9, LFP-8, LFP-7, and LFP-6 composites at a voltage range of 1.0–4.2 V at 0.1C. It can be seen from Fig. 7 that the charge-discharge curve of $LiFePO_4/C-Li_4Ti_5O_{12}$ composite combines the characteristics of charge and discharge curves of $LiFePO_4/C$ and

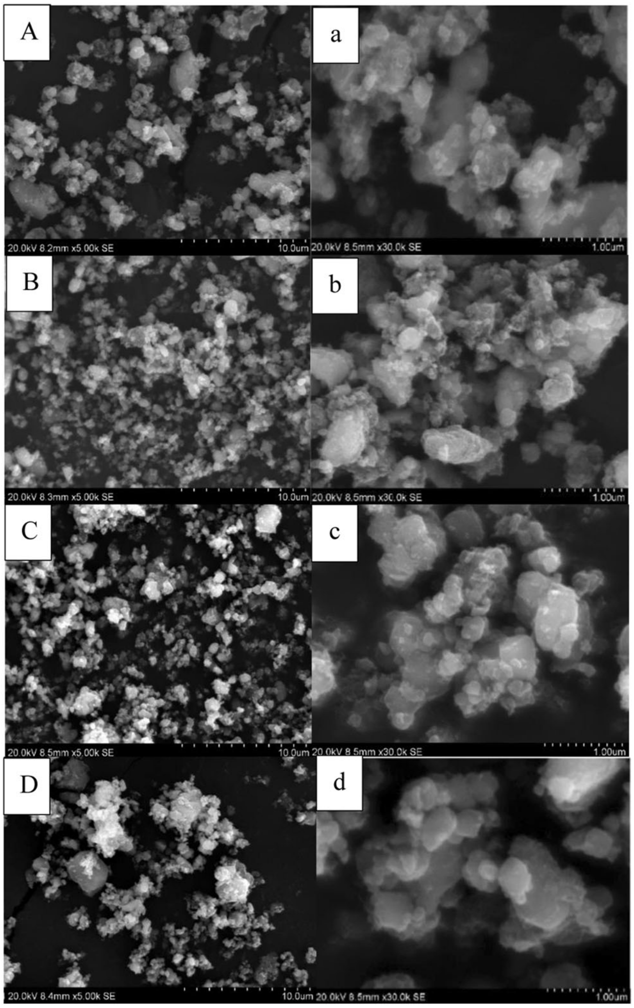

Fig. 4 SEM of LFP-9 (A, a), LFP-8 (B, b), LFP-7 (C, c), and LFP-6 (D, d) samples

$Li_4Ti_5O_{12}$ materials. During the charging process, a platform appears at about 1.5 V, corresponding to the lithium intercalation process of $Li_4Ti_5O_{12}$ material, and another platform appears at 3.5 V, corresponding to the lithium intercalation process of $LiFePO_4$/C material. Subsequent discharges exhibit similar voltage curves, indicating that the material has reversible structural changes during lithium ion insertion and removal. At 0.1C rate, the initial discharge-specific capacities of LFP-9, LFP-8, LFP-7, and LFP-6 composites are 147, 152, 149, and 142 mAh g^{-1}. Comparing $LiFePO_4$/C samples, the specific discharge capacity of the composite is higher than that of the single $LiFePO_4$/C material, because $Li_4Ti_5O_{12}$ is also involved in the electrochemical reaction in the composite. Since the two materials have the first irreversible capacity loss, the coulomb effect of the $Li_4Ti_5O_{12}$ material is higher than that of $LiFePO_4$/C at the same rate. Therefore, the first coulomb efficiency of the composite electrode is higher than that of the single $LiFePO_4$/C material. Among them, LFP-8 material exhibits the highest discharge-specific capacity and superior discharge efficiency.

Cycle performance test

Figure 8 is a cycle curve of single $LiFePO_4$/C, LFP-9, LFP-8, LFP-7, and LFP-6 composites cycled at 0.1C for 100 times. After cycles, the capacity retention rates of single $LiFePO_4$/C and composite materials LFP-9, LFP-8, LFP-7, and LFP-6 are 89.3, 96.5, 97.3, 96.5, and 96.1%, respectively. In comparison, the $LiFePO_4$/C sample has poor cycle performance. The discharge capacity decay rate reaches 10.7% after 100 charge and discharge cycles. As can be seen from the curve, the cycle performance of $LiFePO_4$/C-$Li_4Ti_5O_{12}$ composite is better than that of single $LiFePO_4$/C material. This is because $Li_4Ti_5O_{12}$ has better cycling performance which plays a vital role in improving the cycle performance of $LiFePO_4$/C-$Li_4Ti_5O_{12}$ composite. When the recombination ratio is 8:2, the capacity retention ratio is 97.3%.

Cyclic voltammetry

Figure 9 shows the cyclic voltammetry of $LiFePO_4$/C and $Li_4Ti_5O_{12}$ materials measured at a scan speed of 0.1 mV s^{-1}. The corresponding scan voltage ranges are 2.0–4.6 and 1.0–2.3 V, respectively. We can see that two pairs of symmetry oxidation/reduction peak appear on the curve, which correspond to the deintercalation and intercalation process of Li^+. Figure 9 shows the potential difference between the oxidation potential and the reduction potential of $LiFePO_4$ is 0.42 V, indicating there is a certain polarization phenomenon during the electrode reaction. It is observed that the area of the oxidation peak is larger than the area of the reduction peak. In the process of charge and discharge, the discharge-specific capacity is larger than the charge-specific capacity, and on the cyclic voltammogram, the area of the reduction peak is larger than that of the oxidation peak. The equilibrium potential of Ti^{4+}/Ti^{3+} in $Li_4Ti_5O_{12}$ is 1.55 V. As we can see in the figure, the peak potential of the oxidation peak during charging is greater than the equilibrium potential, while the peak potential of the reduction peak during the discharge is less than equilibrium. The potential difference between the oxidation potential and the reduction potential is 0.35 V, which is significantly smaller than the $LiFePO_4$ potential difference, indicating the polarization of the $Li_4Ti_5O_{12}$ material is smaller than that of $LiFePO_4$. It is observed that the oxidation peak area and the reduced peak area of $Li_4Ti_5O_{12}$ are basically the same, indicating the irreversible capacity loss of this material is less in the charging and discharging process.

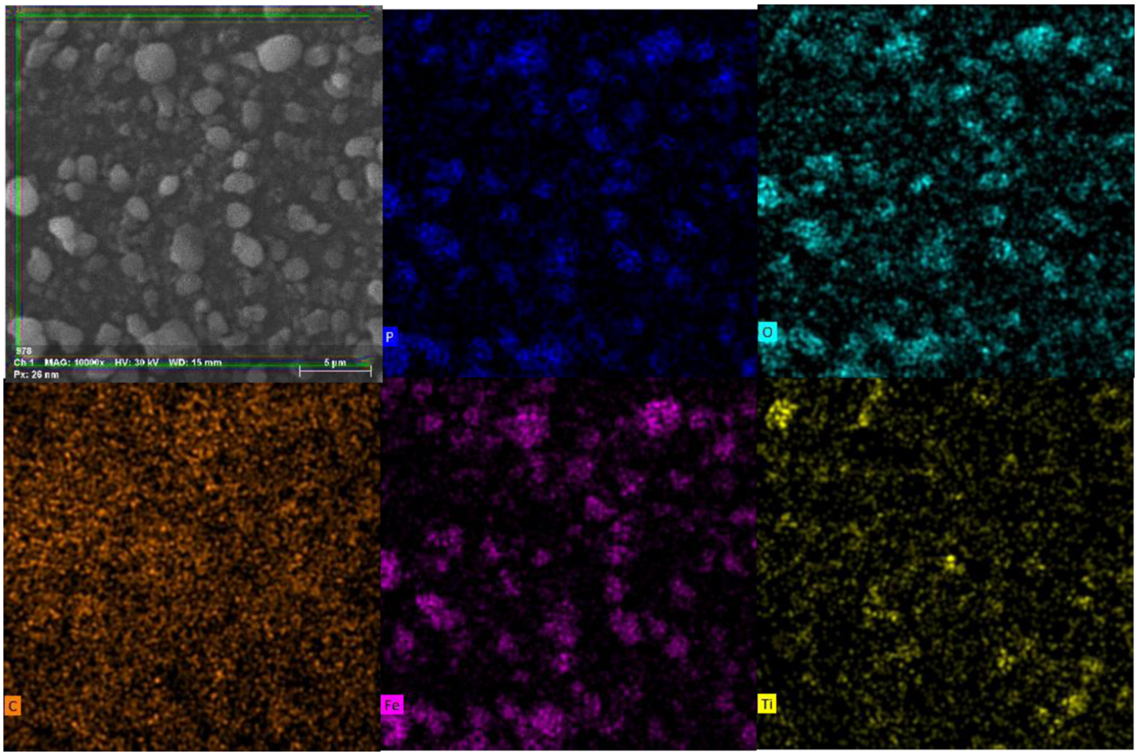

Fig. 5 The EDS diagrams of synthesized material LFP-8

Figure 10 shows the cyclic voltammogram of LFP-9, LFP-8, LFP-7, and LFP-6 composite samples at room temperature with a scan speed of 0.1 mV s^{-1}. The voltage is between 1.0 and 4.2 V. As can be seen from the figure, there are two pairs of redox peak pairs appearing on the curve. The redox peak pair at the low voltage corresponds to intercalation and deintercalation of Li$^+$ in $Li_4Ti_5O_{12}$ material. The redox peak pair at the high voltage is derived from the redox reaction of Fe^{2+}/Fe^{3+} in $LiFePO_4$ material. The peak potential difference between the redox peaks reflects the degree of reversibility of the electrochemical, and the peak current density reflects the electrochemical reaction rate. When the blending ratio is 9:1 (LFP-9), the symmetry between the oxidation peak and the reduction peak is the best. The potential difference is the smallest. This shows that the polarization of the battery is minimum under the blend ratio while the discharge efficiency of the battery and

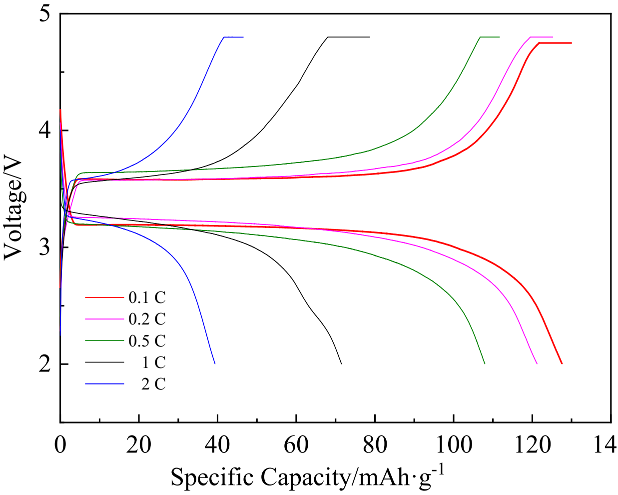

Fig. 6 The first charge-discharge capacity curves of $LiFePO_4$/C samples under different ratios

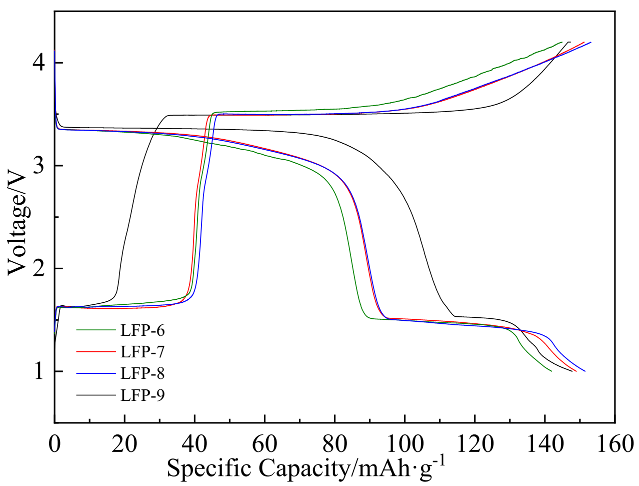

Fig. 7 The first charge-discharge capacity of LFP-9, LFP-8, LFP-7, and LFP-6 composite samples

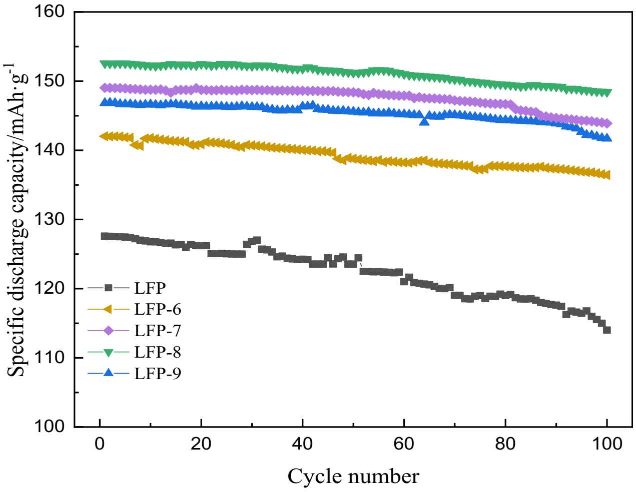

Fig. 8 The cycle curves of $LiFePO_4/C$, $Li_4Ti_5O_{12}$, LFP-9, LFP-8, LFP-7, and LFP-6 materials under 0.1C ratio

the reversibility of the battery is optimal. The charge and discharge amount of the battery is the largest when the blending ratio is 8:2 (LFP-8). This is consistent with the conclusions from the previous charge and discharge test results.

Electrochemical impedance spectroscopy analysis

Figure 11 shows the EIS and equivalent circuit of $LiFePO_4/C$, $Li_4Ti_5O_{12}$, LFP-9, LFP-8, LFP-7, and LFP-6 materials. The frequency range of the test is 1×10^{-2}–1×10^5 Hz. The diameter of the semicircle reflects the charge transfer resistance (R_{ct}) of the electrode. The semicircle of the high-frequency region to the intermediate-frequency region reflects the internal resistance (R_{SEI}) caused by the solid electrolyte membrane on the electrode surface. R_W stands for Warburg resistance, R_S is the resistance of the electrolyte and other ohmic contact resistance in the cell. C_{PE1} and C_{PE2} are the capacitors corresponding to R_{SEI} and R_{ct}.

As can be seen from the figure, the impedance of $Li_4Ti_5O_{12}$ material is much smaller than that of other materials, while the impedance of $LiFePO_4/C$ material is much larger than that of other materials. It is shown that $Li_4Ti_5O_{12}$ material is easier to overcome the dynamic charge binding during charge and discharge, which is more conducive to Li^+ intercalation and deintercalation, while $LiFePO_4/C$ material is relatively difficult. The impedance of the composite is lower than that of single $LiFePO_4/C$ after the two materials are combined. The results show that the addition of $Li_4Ti_5O_{12}$ has a positive effect on the reduction of material resistance, improving the migration ability of Li^+ and promoting the electrochemical performance.

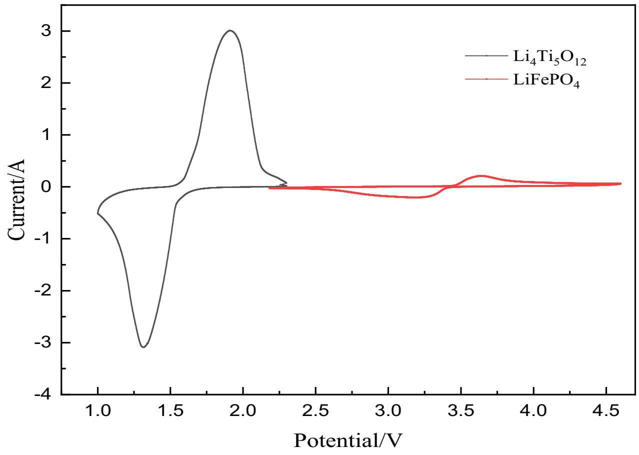

Fig. 9 The CV curves of $LiFePO_4/C$ and $Li_4Ti_5O_{12}$ materials

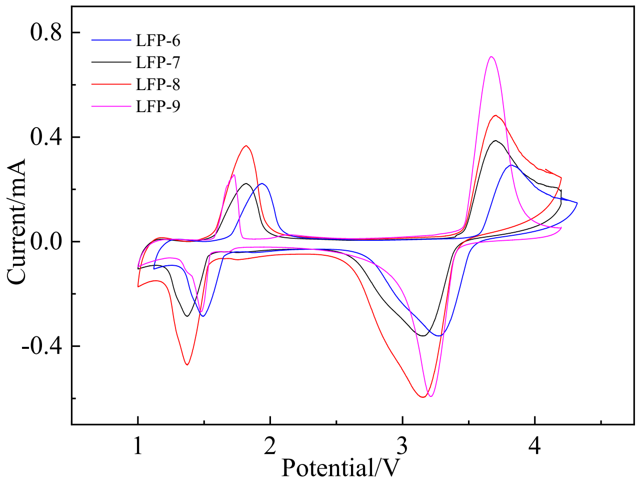

Fig. 10 The CV curves of LFP-9, LFP-8, LFP-7, and LFP-6 composite materials under different composite ratios

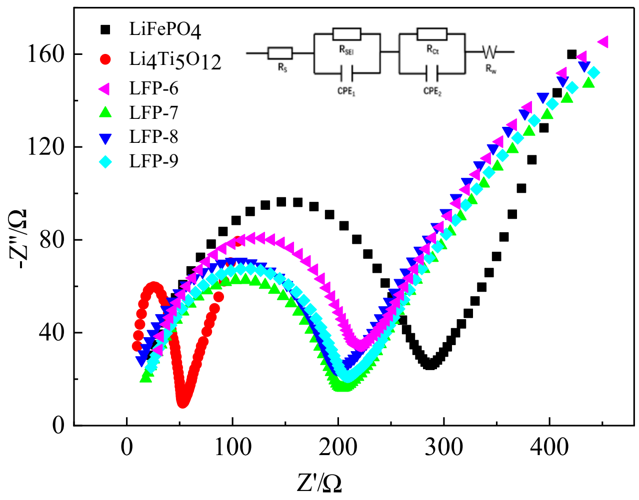

Fig. 11 The EIS curves and equivalent circuit of $LiFePO_4/C$, $Li_4Ti_5O_{12}$, LFP-9, LFP-8, LFP-7, and LFP-6 materials

Conclusions

Lithium-ion batteries have the advantages of high energy density, large charge and discharge current, and long cycle life, making them the most competitive and promising power source in this century. The improved method of this experiment effectively improves the electrochemical performance of $LiFePO_4$.

The sample with the recombination ratio was 8:2 showed best electrochemical performance. The obtained composite material had fine particles and uniform size. In summary, compared with single $LiFePO_4$, the electrochemical performance of $LiFePO_4/C\text{-}Li_4Ti_5O_{12}$ composites was superior, which promoted the development of $LiFePO_4$ cathode materials and accelerates its practical development.

Funding information This work was supported by Program for Liaoning Innovation Talents in University and Liaoning Provincial Natural Science Foundation of China (No.20170540776).

References

1. Wen YX, Zheng MP, Tong ZF (2005) Effect of Ni_{2+} ion doping on performance and structure of lithium iron phosphate. Trans Nonferrous Met Soc China 09:1436–1440
2. Sehrawat R, Sil A (2015) Effect of solvents on electrochemical performance of polypyrrole coated $LiFePO_4/C$ cathode materials for Li-ion battery. J Mater Sci Mater Electron 26(7):5175–5185
3. Zaghib K, Dontigny M, Perret P, Guerfi A, Ramanathan M, Prakash J, Mauger A, Julien CM (2014) Electrochemical and thermal characterization of lithium titanate spinel anode in $C\text{-}LiFePO_4//C\text{-}Li_4Ti_5O_{12}$ cells at sub-zero temperatures [J]. J Power Sources 248:1050–1057
4. Huang YW, He Y, Howard S, Lu X, Dong HN, Sudeshna S, Dong HL, Li XF, Duck YK, Mao H-K, Liu YZ, Li HP, Li H, Wang L (2019) Li-ion battery material under high pressure: amorphization and enhanced conductivity of $Li_4Ti_5O_{12}$. Natl Sci Rev 6(02):239–246
5. Zhang KJ, Chen P, Xie WW, Cai J, Zhou ZP (2018) Progress in modification of lithium iron phosphate and its advantages and disadvantages. Inorg Chem Ind 50(06):13–17
6. Xu X (2018) Effect of Ti content on the properties of doped lithium iron phosphate cathode materials. Anhui Chem Ind 44(06):67–69
7. Luo GE, Liu WJ, Yu XY (2013) Effect of pyrrole additive on structure and properties of $LiFePO_4/C$ cathode materials prepared by in situ polymerization restriction method. J Chin Ceram Soc 41(1):19–23(5)
8. Yeonju P, Min KS, Sila X, Man LS, Isao N, Mee JY (2019) Investigation of the phase transition mechanism in $LiFePO_4$ cathode using in situ raman spectroscopy and 2D correlation spectroscopy during Initial cycle. Molecules 24(2):291
9. Cao Y, Li Q, Lou SF, Ma YL, Du CY, Gao YZ, Yin GP (2018) Enhanced electrochemical performance of $Li_4Ti_5O_{12}$ through in-situ coating $70Li_2S\text{-}30P_2S_5$ solid electrolyte for all-solid-state lithium batteries. J Alloys Compd 752:8–13
10. Qin GH (2017) The preparation of $LiFePO_4$ material and its application in lithium ion batteries. Tianjin University 1–8 (In Chinese)
11. Wei XF (2018) Study on the improvement of rate performance of $LiFePO_4$ cathode material by graphene. Beijing University of Chemical Technology 2–14 (In Chinese)
12. Xi YK (2018) Structural modulation and electrochemical performance of lithium ion battery cathode materials. Shanghai Institute of Technology 3–8 (In Chinese).
13. Tan YK (2018) The preparation and properties investigation of $LiFePO_4$ modified by nano-carbon materials as Lithium Ion Battery Cathode materials. Central South University of Forestry and Technology.
14. Wang XD, Zhang CL, Wang SW, Wu DP, Guo XH, Liu ZX, Yu X (2017) Investigation on the preparation and performance of lithium iron phosphate battery with binary saccharide-based carbon source. New Chemical Materials 45(12):103–106
15. Lin YC, Fey GT, Wu PJ, Chang JK, Kao HM (2013) Synthesis and electrochemical properties of $\chi LiFePO_4 \cdot (1\text{-}\chi)LiVPO_4F$ composites prepared by aqueous precipitation and carbothermal reduction. J Power Sources 244:63–71
16. Omenya F, Chernova NA, Upreti S, Zavalij PY (2011) Can vanadium be substituted into $LiFePO_4/C$? Chem Mater 23(21):4733–4740
17. Yang K, Deng Z, Suo J (2012) Effects of carbon sources and carbon contents on the electrochemical properties of $LiFePO_4/C$ cathode material. J Solid State Electrochem 16(8):2805–2813
18. Hoang K, Johannes MD (2012) First-principles studies of the effects of impurities on the ionic and electronic conduction in $LiFePO_4$. J Power Sources 206:274–281
19. Tang ZY, Yang XX, Chen YH, He YB (2007) Research progress on electrode material lithium titanate. Chinese J Power Sources 31(4):332–336
20. Cui W (2011) Electrochemical performance and safety evaluation of $LiFePO_4/Li_4Ti_5O_{12}$ lithium ion battery. Tianjin University 1–23 (In Chinese)
21. Hu JT, Zheng JX, Pan F (2019) Research progress into the structure and performance of $LiFePO_4$ cathode materials. Acta Physico-Chimica Sinic 35(04):361–370
22. Wang X (2018) Study on the Performance of recovery and regeneration from LiFePO4 Cathode Scraps. Xiangtan University 13–26 (In Chinese)
23. Naik A, Zhou J, Gao C, Wang L (2014) Microwave synthesis of $LiFePO_4$ from iron carbonyl complex. Electrochim Acta 142:215–222
24. Zhang AL (2018) Synthesis and performance of Nb^{5+}-Doped $LiFePO_4/C$ as cathode material in lithium-Ion battery. Int J Electrochem Sci:5243–5252
25. Yuan LX, Wang ZH, Zhang WX, Hu XL (2011) Development and challenges of $LiFePO_4$ cathode material for lithium-ion batteries. Energy Environ Sci 42(1):269–284
26. Doeff MM, Wilcox JD, Yu R, Aumentado A, Marcinek M, Kostecki R (2008) Impact of carbon structure and morphology on the electrochemical performance of LiFePO4/C composites. J Solid State Electrochem 12(7–8):995–1001
27. Satou Y, Komine S, Itou S, Asai H, Yao T, Takai S (2017) Differences between the kinetically preferred states of $LiFePO_4$ during charging and discharging observed using in situ X-ray diffraction measurements. J Electrochem Soc 164(6):1281–1284
28. Liu YY, Gu JJ, Zhang JL, Yu F (2015) $LiFePO_4$ nanoparticles growth with preferential (010) face modulated by Tween-80. RSC Adv 5(13):9745–9751
29. Noh MH, Thivel PX, Lefrou C, Bultel Y (2016) Fast-charging of lithium iron phosphate battery with ohmic-drop compensation method. J Energy Storage 8:160–167

30. Lu JJ, Li WL, Shen C, Tang DM, Dai LX, Diao GW, Chen M (2019) Nano-scale hollow structure carbon-coated $LiFePO_4$ as cathode material for lithium ion battery. Ionics 25(9):4075–4082
31. Yamada A, Chung SC, Hinokuma K (2010) Optimized $LiFePO_4$ for lithium battery cathodes. Cheminform 32(29): 17–17
32. Rao Y, Wang K, Zeng H (2014) The effect of phenol–formaldehyde resin on the electrochemical properties of carbon-coated $LiFePO_4$ materials in pilot scale. Ionics 21(6):1525–1531
33. Lin Y, Wu JB, Yu YB (2010) Excessive iron Source on the structural and electrochemical properties of $LiFePO_4$/C composite. Adv Mater Res 123–125(2):1227–1230
34. Mi CH, Zhang XG, Zhao XB, Li HL (2006) Effect of sintering time on the physical and electrochemical properties of $LiFePO_4$/C composite cathodes. J Alloys Compd 424(1–2):327–333